

 Open access • Journal Article • DOI:10.1021/JACS.7B09934

Molecular and Silica-Supported Molybdenum Alkyne Metathesis Catalysts: Influence of Electronics and Dynamics on Activity Revealed by Kinetics, Solid-State NMR, and Chemical Shift Analysis. — [Source link](#)

Deven P. Estes, Christopher P. Gordon, Alexey Fedorov, Wei-Chih Liao ...+10 more authors

Institutions: ETH Zurich, Braunschweig University of Technology, University of Oslo, University of Montpellier

Published on: 20 Nov 2017 - Journal of the American Chemical Society (American Chemical Society)

Topics: Alkyne metathesis, Carbon-13 NMR, Solid-state nuclear magnetic resonance, Alkyne and Reactivity (chemistry)

Related papers:

- [Alkyne metathesis on the rise.](#)
- [Tuning the Catalytic Alkyne Metathesis Activity of Molybdenum and Tungsten 2,4,6-Trimethylbenzylidyne Complexes with Fluoroalkoxide Ligands OC\(CF₃\)_nMe_{3-n} \(n = 0–3\)](#)
- [Practical new silyloxy-based alkyne metathesis catalysts with optimized activity and selectivity profiles.](#)
- [Well-Defined Alkyne Metathesis Catalysts: Developments and Recent Applications](#)
- [Alkyne Metathesis with Silica-Supported and Molecular Catalysts at Parts-per-Million Loadings](#)





Share this paper:    

View more about this paper here: <https://typeset.io/papers/molecular-and-silica-supported-molybdenum-alkyne-metathesis-iklfd3mg9>

Molecular and Silica-Supported Molybdenum Alkyne Metathesis Catalysts: Influence of Electronics and Dynamics on Activity Revealed by Kinetics, Solid-State NMR and Chemical Shift Analysis

Journal Article

Author(s):

Estes, Deven P.; [Gordon, Christopher](#) ; [Fedorov, Alexey](#) ; Liao, Wei-Chih; Ehrhorn, Henrike; Bittner, Celine; Zier, Manuel L.; Bockfeld, Dirk; [Chan, Ka Wing](#) ; Eisenstein, Odile; Raynaud, Christophe; Tamm, Matthias; [Copéret, Christophe](#) 

Publication date:

2017-12-06

Permanent link:

<https://doi.org/10.3929/ethz-b-000210999>

Rights / license:

[In Copyright - Non-Commercial Use Permitted](#)

Originally published in:

Journal of the American Chemical Society 139(48), <https://doi.org/10.1021/jacs.7b09934>

Funding acknowledgement:

150709 - High-Throughput Experimentation (HTE) platform at ETH Zürich (SNF)
169134 - Molecular Approach to Heterogeneous Catalysis (SNF)

Molecular and Silica-Supported Molybdenum Alkyne Metathesis Catalysts: Influence of Electronics and Dynamics on Activity Revealed by Kinetics, Solid-State NMR and Chemical Shift Analysis

Deven P. Estes,^{‡†[a]} Christopher P. Gordon,^{‡[a]} Alexey Fedorov,^[a] Wei-Chih Liao,^[a] Henrike Ehrhorn,^[b] Celine Bittner,^[b] Manuel Luca Zier,^[b] Dirk Bockfeld,^[b] Ka Wing Chan,^[a] Odile Eisenstein,^[c, d] Christophe Raynaud,^[c] Matthias Tamm,^{*[b]} Christophe Copéret*^[a]

^[a] Department of Chemistry and Applied Biosciences, ETH Zürich, Vladimir-Prelog-Weg 1-5, 8093 Zürich, Switzerland

^[b] Institut für Anorganische und Analytische Chemie, Technische Universität Braunschweig, Hagenring 30, 38106 Braunschweig, Germany

^[c] Institut Charles Gerhardt, UMR 5253 CNRS-UM-ENSCM, Université de Montpellier, Place E. Bataillon, F-34095 Montpellier, France

^[d] Hylleraas Centre for Quantum Molecular Sciences, Department of Chemistry, University of Oslo, P.O. Box 1033, Blindern, 0315 Oslo, Norway

KEYWORDS Alkyne Metathesis, Molybdenum Alkylidyne, Fluorinated Alkoxide, Metallacyclobutadiene, Surface Organometallic Chemistry, NMR shielding tensor, Two-component DFT/ZORA calculations

ABSTRACT: Molybdenum-based molecular alkylidyne complexes of the type [MesC≡Mo{OC(CH₃)₃]₃-x(CF₃)_x]₃ (**MoF**₀, x = 0; **MoF**₃, x = 1; **MoF**₆, x = 2; **MoF**₉, x = 3; Mes = 2,4,6-trimethylphenyl) and their silica-supported analogues are prepared, characterized at the molecular level, in particular by solid-state

NMR, and their alkyne metathesis catalytic activity is evaluated. The ^{13}C NMR chemical shift of the alkyldiyne carbon increases with increasing number of fluorine atoms on the alkoxide ligands for both molecular and supported catalysts, however, with more shielded values for the supported complexes. The activity of these catalysts increases in the order $\text{MoF}_0 < \text{MoF}_3 < \text{MoF}_6$ before sharply decreasing for MoF_9 , with a similar effect for the supported systems ($\text{MoF}_0 \approx \text{MoF}_9 < \text{MoF}_6 < \text{MoF}_3$). This is consistent with the different kinetic behavior (0^{th} order in alkyne for MoF_9 derivatives instead of 1^{st} order for the others) and the isolation of stable metallacyclobutadiene intermediates of MoF_9 for both molecular and supported species. Detailed solid-state NMR analysis of molecular and silica-supported metal alkyldiyne catalysts coupled with DFT/ZORA calculations rationalize the NMR spectroscopic signatures and discernable activity trends at the frontier orbital level: 1) increasing the number of fluorine atoms lowers the energy of the $\sigma^*(\text{M}\equiv\text{C})$ orbital, explaining the more deshielded chemical shift values; it also leads to an increased electrophilicity and higher reactivity for catalysts up to MoF_6 , prior to a sharp decrease in reactivity for MoF_9 due to the formation of stable metallacyclobutadiene intermediates and 2) the silica-supported catalysts are less active than their molecular analogues because they are less electrophilic and dynamic, as revealed by their ^{13}C NMR chemical shift tensors.

Introduction

While the past 2-3 decades have seen remarkable advances in olefin metathesis,¹⁻⁵ the progress in related alkyne metathesis has gained momentum more recently.⁶⁻¹³ Several efficient Schrock-type alkyldiyne catalysts having the general formula $[\text{RC}\equiv\text{M}(\text{X})_3]$ ($\text{M} = \text{Mo}$ or W) have been developed (Chart 1),¹⁴⁻¹⁶ featuring a range of ancillary X-type ligands including fluorinated alkoxides,¹⁷⁻²² chelating phenoxides,²³⁻²⁵ siloxides,²⁶⁻³⁰ as well as amido ligands and combinations thereof.^{8, 17, 31-32} The development of efficient catalysts has led to applications of alkyne metathesis in reactions such as polymerization,³³⁻³⁵ cross-metathesis, and ring-closing alkyne metathesis (RCAM), which has been utilized in natural product and polymer synthesis.^{7, 13, 36-43}

Despite these advances, alkyne metathesis catalysts would still benefit from improved activity and stability. Several deactivation mechanisms have been identified such as the bimolecular elimination of alkyne,⁴⁴ the formation of metallatetrahydrane species⁴⁵⁻⁴⁷ or cyclopentadienyl species,⁴⁵ as well as, in the case of terminal alkynes, deprotonation of the intermediate metallacyclobutadienes, resulting in polymerization.^{7, 14-16} One strategy to increase the stability of molecular catalysts is to use the surface organometallic chemistry (SOMC) approach. For instance, grafting of catalysts on the isolated surface $\equiv\text{SiOH}$ groups of partially dehydroxylated silica generates well-defined silica-supported metal complexes, suppressing bimolecular deactivation pathways.⁴⁸ In these catalysts, the loading of the active species is mostly controlled by the surface coverage of $\equiv\text{SiOH}$ groups, which is in turn controlled by the pre-treatment temperature of the silica support.⁴⁹ This SOMC approach has allowed the development of highly efficient alkene metathesis catalysts, having performance exceeding in many instances their homogeneous analogues.⁵⁰⁻⁵² A similar approach has been used to prepare the corresponding alkyne metathesis catalysts.⁵³⁻⁵⁸ In particular, we recently reported that $\text{MesC}\equiv\text{Mo}(\text{OC}(\text{CH}_3)(\text{CF}_3)_2)_3$ ($\text{MesC}\equiv\text{Mo}(\text{OtBuF}_6)_3$ or MoF_6) grafts onto silica partially dehydroxylated at 700 °C (SiO_{2-700}) producing $\text{MesC}\equiv\text{Mo}(\text{OtBuF}_6)_2(\text{OSi}\equiv)$ species ($\text{MoF}_6/\text{SiO}_{2-700}$, Chart 1) to provide a highly active catalyst.⁵⁸ Both the molecular and the grafted catalyst featured a remarkable performance in the self-metathesis of carefully purified 1-phenyl-1-propyne, with MoF_6 achieving turnover numbers (TONs) and turnover frequencies (TOFs) of up to 185,000 and 188 s⁻¹, respectively. These catalysts could also efficiently promote RCAM as well as cross metathesis of terminal alkynes under mild conditions.⁵⁸ Notably, $\text{MoF}_6/\text{SiO}_{2-700}$ shows much lower activity in these reactions than the corresponding molecular precursor MoF_6 even if both achieved high TONs.

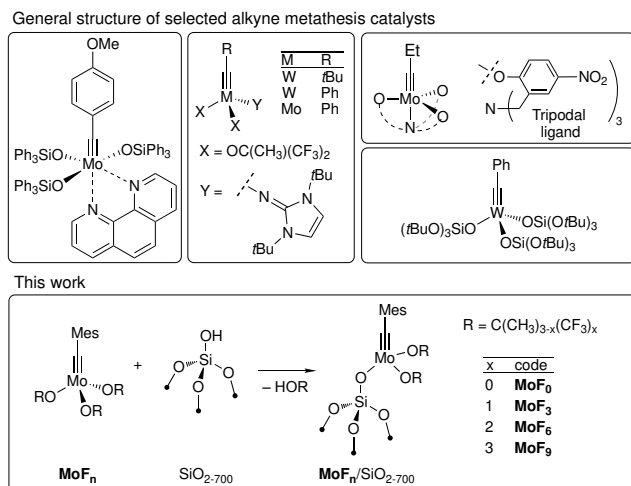


Chart 1. State of the art and the studied catalysts of this work.

In parallel to what is known in Schrock-type olefin metathesis catalysts, one can reason that tuning the electronic and the steric properties of the X-type ligands can tune the activity and the stability of the catalyst. In fact, similar to findings in olefin metathesis,^{51, 59-61} tuning the electronic properties of alkoxide ligands by introducing fluorine as in $\text{MesC}\equiv\text{Mo}\{\text{OC}(\text{CH}_3)_{3-x}(\text{CF}_3)_x\}_3$, where $x = 0, 1, 2, 3$, (**MoF_n**, $n = 0, 3, 6, 9$), dramatically influences the efficiency of these alkyne metathesis catalysts, **MoF₆** providing the best catalytic performances (highest TOFs and TONs) and **MoF₉**, showing particularly low TOFs.⁶²⁻⁶³ However, it is not clear why **MoF₆** shows a peak in activity and how the corresponding silica-supported systems would perform in catalysis.

Here, we investigate the structure-activity relationship in a series of molecular (**MoF_n**) and silica-supported (**MoF_n/SiO₂₋₇₀₀**) alkyne metathesis catalysts as well as in an isostructural molecular model, mimicking the surface silanol by $(t\text{BuO})_3\text{SiOH}$ in **MoF₆-TBOS**, which entails detailed kinetic studies and investigation of reaction intermediates for both molecular and supported systems. Combined with solid-state NMR spectroscopy and computational DFT studies including Natural Chemical Shift (NCS) analysis, we investigate the effect of the ligand and the surface on the structure and the dynamics of pre-catalyst and reaction intermediates in relation with their catalytic performances.

Results and Discussion

Preparation and Characterization of Silica-Supported Molybdenum 2,4,6-Trimethylbenzylidyne Complexes.

The silica-supported catalysts $\text{MoF}_n/\text{SiO}_{2-700}$ ($n = 0, 3$ and 9) are prepared using a Surface Organometallic Chemistry (SOMC)⁵¹ approach by grafting the respective MoF_n on silica partially dehydroxylated at 700°C under vacuum, as previously reported for MoF_6 (Chart 1).⁵⁸ Reaction of the molecular species with silica produces the corresponding grafted Mo species along with the respective free alcohol in solution that is quantified by NMR spectroscopy (see Supporting Information for details). Reaction of the molecular complexes on the surface is evidenced by a decrease in intensity of the O–H stretching band originating from the isolated silanols (Figures S10) and the appearance of new C–H stretching and bending bands in the IR spectrum of the surface species. In addition, a small broad band appears at 3600 cm^{-1} , which indicates that some residual OH groups interact with the grafted organometallic fragments.⁶⁴ The amount of Mo on the surface according to elemental analysis is $0.24, 0.18,$ and $0.20\text{ mmol Mo g}^{-1}$ for $\text{MoF}_0, \text{MoF}_3$ and $\text{MoF}_9/\text{SiO}_{2-700}$, respectively (Table 1), similarly to what is obtained for $\text{MoF}_6/\text{SiO}_{2-700}$ ($0.16\text{ mmol Mo g}^{-1}$). C, H, and F elemental analysis compared to the amount of Mo on the surface is typically within error of the expected structure $[\text{MesC}\equiv\text{Mo}\{\text{OC}(\text{CH}_3)_{3-x}(\text{CF}_3)_x\}_2(\text{OSi}\equiv)]$, the exception being the somewhat low C and F elemental analysis for MoF_0 and MoF_9 , respectively. The lower than expected C and F content can be associated with the formation of MoC during the analysis and the difficulties of performing analysis of F in silica samples, respectively.

Table 1. Elemental analysis of silica-supported catalysts (errors calculated from the standard error tolerance of elemental analysis are given in parenthesis).

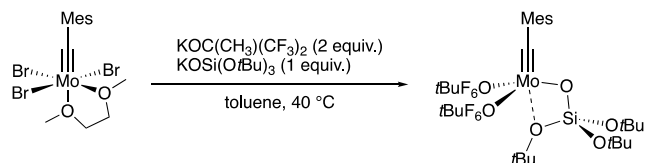
Species	% Mo	C/Mo	H/Mo	F/Mo
$\text{MoF}_0/\text{SiO}_{2-700}$	2.32	13(2)	20(17)	—
$\text{MoF}_3/\text{SiO}_{2-700}$	1.71	17(2)	22(23)	9(3)

MoF₆/SiO₂₋₇₀₀	1.76	19(2)	19(20)	11(3)
MoF₉/SiO₂₋₇₀₀	1.94	17(2)	13(20)	11(3)

We also characterized the **MoF_n/SiO₂₋₇₀₀** surface species by ¹H, ¹⁹F, and ¹³C MAS NMR (Figures S11-S21). The ¹H NMR spectra of all these species show resonances corresponding to the mesityl- and *t*BuF_nO-fragments, except for **MoF₉/SiO₂₋₇₀₀**, which has no proton on the alkoxide ligand. The ¹⁹F NMR of **MoF₉/SiO₂₋₇₀₀** showed a single peak corresponding to the CF₃ groups of the *t*BuF₉ fragment (-75.9 ppm). However, the ¹⁹F NMR of **MoF₃/SiO₂₋₇₀₀** showed three peaks, two corresponding to two different CF₃ groups (-81.5 and -86.5 ppm), and one downfield signal at -145 ppm. This latter signal may be due to formation of Si-F groups on the surface, which has been observed to have very similar chemical shifts.⁶⁵⁻⁶⁶ Similarly, **MoF₆/SiO₂₋₇₀₀** showed two resonances in the ¹⁹F NMR (-83.5 and -84.8 ppm), attributed to the diastereotopic CF₃ groups of the ligand.⁵⁸ While ¹³C NMR signals could be obtained for all species for the mesityl and *t*BuF_nO- fragments, neither direct detection nor cross-polarization techniques revealed an alkyldiyne signal. However, the ¹³C NMR alkyldiyne signal of **MoF₆/SiO₂₋₇₀₀** was studied by grafting the corresponding ¹³C labeled precursor. This yielded a silica-supported labeled alkyldiyne that could be observed by solid state NMR with an isotropic chemical shift of 301 ppm, significantly more shielded than the molecular precursor (317 ppm).⁵⁸

For further understanding this silica-supported system, we also prepared the molecular analogue, [MesC≡Mo{OC(CH₃)(CF₃)₂}₂(OSi(*Ot*Bu)₃)] (**MoF₆-TBOS**) from [MesC≡MoBr₃(dme)] by reaction with two equivalents of the alkoxide KOC(CH₃)(CF₃)₂ and one equivalent of the silanolate KOSi(*Ot*Bu)₃ in toluene at 40 °C (Scheme 1). Complex **MoF₆-TBOS** could be obtained as a yellow crystalline solid in 70% yield.

Scheme 1. Synthesis of **MoF₆-TBOS**.



The ^{13}C NMR spectrum of **MoF₆-TBOS** exhibits a characteristic low field signal at 306.6 ppm for the alkylidyne carbon atom, which is upfield compared to **MoF₆** (317.6 ppm), but slightly downfield compared to **MoF₆/SiO₂₋₇₀₀** (301 ppm). Introduction of the silanolate ligand renders the complex *C_s* symmetric, and accordingly, two quartets at -77.1 and -77.6 ppm with $^4J_{\text{FF}} = 9$ Hz are observed in the ^{19}F NMR spectrum for diastereotopic CF_3 groups. An ORTEP diagram of the X-ray crystal structure is shown in Figure 1. The complex crystallizes in the monoclinic space group $P2_1/n$. Similar to other 2,4,6-trimethylbenzylidyne complexes, the Mo atom resides in a distorted tetrahedral environment with a short Mo-C1 bond of 1.755(3) Å and three Mo-O bonds of ca. 1.91 < Å. In addition, the TBOS ligand binds in a chelating fashion through the oxygen atom O4 of one of the Si-O*t*Bu groups, affording a significantly longer Mo-O4 bond distance of 2.5734(16) Å.

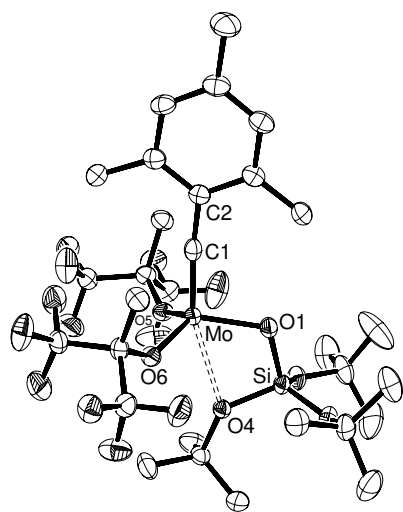


Figure 1. ORTEP diagram of **MoF₆-TBOS** with thermal displacement parameters drawn at 50% probability. Selected bond lengths [Å] and angles [°]: Mo-C1 1.755(3), Mo-O1 1.9223(16), Mo-O5 1.9079(17), Mo-O6 1.9040(17), Mo-O4 2.5734(16), Mo-C1-C2 173.5(2)

In order to further investigate the structure of the surface-supported species $\text{MoF}_6/\text{SiO}_{2-700}$, the three representative and most active (*vide infra*) alkyne metathesis catalysts MoF_6 , $\text{MoF}_6\text{-TBOS}$ and $\text{MoF}_6/\text{SiO}_{2-700}$ were also analyzed by K-edge XANES spectroscopy (Tables 2, S2-S4, and Figures S28-S31). All three species show a nearly identical edge position and very similar pre-edge features, indicating that they have similar geometries and the same oxidation state. Notably, the XANES spectrum of $\text{MoF}_6/\text{SiO}_{2-700}$ is almost identical to molecular MoF_6 , while molecular $\text{MoF}_6\text{-TBOS}$ exhibits an additional feature at ca. 20039.5 eV suggesting a slightly different coordination environment as compared to the other two species. Analysis of the EXAFS region in R space indicates the expected alkylidyne carbon and three oxygens in all cases. For MoF_6 , besides the short $\text{Mo}\equiv\text{C}$ distance (1.73(1) Å; 1.744 Å in X-ray structure) and the three oxygens at 1.923(3) Å (1.895 to 1.924 Å in X-ray),¹⁹ additional interactions associated with a fluorine atom in the second coordination sphere improve the fit, consistent with the X-ray structure (2.81(3) Å; 2.738 Å in X-ray). For $\text{MoF}_6\text{-TBOS}$, EXAFS fitting analysis are consistent with a slightly elongated $\text{Mo}\equiv\text{C}$ distance (1.74(1) Å; 1.755 Å in X-ray), three oxygens at 1.934(5) Å (1.904 to 1.922 Å in X-ray) as well as the presence of an additional oxygen at ca. 2.74(3) Å (2.573 Å in X-ray) consistent with the \square^2 -siloxo ligand (Figure 1 and Table 2). Notably, for both MoF_6 and $\text{MoF}_6\text{-TBOS}$, EXAFS predicts a slightly longer distance for the closest atom in the 2nd coordination sphere (F and O respectively) than expected from the X-ray structure, which likely result from the different measurement conditions (room temperature for EXAFS vs. 100 K for X-ray). In fact, according to DFT calculations on $\text{MoF}_6\text{-TBOS}$ there is hardly any energetic difference between a long and a short Mo-O contact (see Table S7). For the grafted species $\text{MoF}_6/\text{SiO}_{2-700}$ the first coordination sphere contains a $\text{Mo}\equiv\text{C}$ at 1.715(8) Å, similarly to what is observed for MoF_6 along with two oxygens at 1.926(5) and one oxygen at 1.915(5) Å. However, no additional oxygen and fluorine interaction is found.

Table 2. Fitted scattering paths from EXAFS measurements. All values are given in Å.

	1 st coord. sphere		2 nd coord. sphere	
	Atom	Distance	Atom	Distance
MoF₆	C (1)	1.73(1)	F (1)	2.81(3)

MoF₆-TBOS	O (3)	1.923(3)	C (2)	3.28 (1)
	C (1)	1.74(1)	O (1)	2.74(3)
MoF₆/SiO₂₋₇₀₀	O (3)	1.934(5)	Si (1)	3.06(3)
	C (1)	1.715(8)	Si (1)	3.12 (2)
	O (2)	1.926(5)		
	O (1)	1.915(5)		

Catalytic Performances and Kinetic Studies.

Next, we evaluated and compared the catalytic performances of these catalysts in the self-metathesis of 1-phenyl-1-propyne at low loadings (25 ppm for molecular and 0.05-0.1 mol% for supported catalysts) in the presence of 5 Å molecular sieves in toluene at 27 °C. The catalyst turn-over frequencies, calculated from the conversion to diphenylacetylene after five minutes (TOF_{5min}), vary between 0.2 and 230 s⁻¹, (Table 3) the activity decreasing in the order **MoF₆ ≈ MoF₆-TBOS > MoF₃ > MoF₀ > MoF₉**, showing the dramatic influence of the ligand. The silica-supported species were significantly less active than the molecular catalysts, as previously found for **MoF₆**.⁵⁸ For the surface species, unlike the molecular species, the trend shows that **MoF₃/SiO₂₋₇₀₀** had slightly higher activity than **MoF₆/SiO₂₋₇₀₀**. Both **MoF₀/SiO₂₋₇₀₀** and **MoF₃/SiO₂₋₇₀₀**, with more electron rich ligands, show deactivation and do not reach equilibrium conversion. However, **MoF₃/SiO₂₋₇₀₀** shows slightly higher initial rate than **MoF₆/SiO₂₋₇₀₀**, but slows down over the course of the reaction, reaching a slightly lower final conversion than **MoF₆/SiO₂₋₇₀₀**. The catalyst **MoF₀/SiO₂₋₇₀₀** achieved only 10% conversion. The order of reactivity for the supported species based on initial TOF is **MoF₃/SiO₂₋₇₀₀ > MoF₆/SiO₂₋₇₀₀ > MoF₀/SiO₂₋₇₀₀ > MoF₉/SiO₂₋₇₀₀**, with TOF_{5min} varying between 0.04 and 0.6 s⁻¹, and showing a volcano-type dependence of activity with the ligand donor properties. In the case of both the supported and molecular catalysts, **MoF₉** was slowest followed by **MoF₀**. Noteworthy is the comparable activity of **MoF₆-TBOS** and **MoF₆** (Figure S27), which contrast drastically with the low activity of **MoF₆/SiO₂₋₇₀₀**. This together with the high anisotropy of the alkylidyne ¹³C chemical shift observed for silica-supported systems at room temperature and the shifted surface-OH stretching band in the IR spectrum (Figure S10, *vide infra*) suggests that the metal fragment (the active

center) interacts strongly with the silica surface in **MoF₆/SiO₂₋₇₀₀**; it implies little dynamics, possibly explaining the low activity.

Table 3. Catalytic activity of molecular (25 ppm) and supported (0.05-0.1 mol%) catalysts for self-metathesis of 1-phenyl-1-propyne (ca. 0.6 M in toluene).

Catalyst	TOF _{5min} (s ⁻¹)	TON (% conv)
MoF₀	10	11400 (29%)
MoF₃	50	38000
MoF₆	230	116000
MoF₆-TBOS	190	127000
MoF₉	0.20	11500 (29%)
MoF₀/SiO₂₋₇₀₀	0.08	90 (7%)
MoF₃/SiO₂₋₇₀₀	0.60	1010
MoF₆/SiO₂₋₇₀₀	0.42	1990
MoF₉/SiO₂₋₇₀₀	0.04	290 (24%)

Reactions monitored at 27 °C in toluene for 6 hours with 5 g of 5 Å activated molecular sieves. Given in parentheses is the conversion when equilibrium was not reached.

The rate laws for **MoF₀**, **MoF₃**, and **MoF₆** are all 1st order in catalyst and 1st order in substrate, as shown by the concentration dependence on conversion (Figure S25). In sharp contrast, the concentration of diphenylacetylene vs. reaction time for **MoF₉** shows an apparent zero-order in substrate (Figure 2) as varying the initial concentration of the substrate by a factor of five produces no difference in the initial rate. However, the plots have a slight curvature at high conversions, suggesting that they are not truly zero-order. This could be caused by rapidly maintained and favorable pre-equilibrium binding of the alkyne to the catalyst before the rate-determining step, which in this case would be loss of 2-butyne from the catalyst, as was previously observed for tungsten alkyne metathesis catalysts.⁴⁶ The situation for **MoF₉** is most likely such that the binding constant is only marginally larger than 1, causing a slight curvature in

the overall concentration vs time plot. Similar effects were observed in the reactions of $\text{MoF}_9/\text{SiO}_{2-700}$ that shows zero-order behavior, while the other catalysts are 1st order (Figure S26).

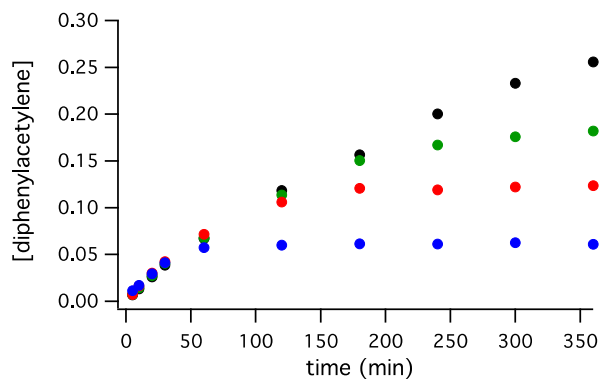


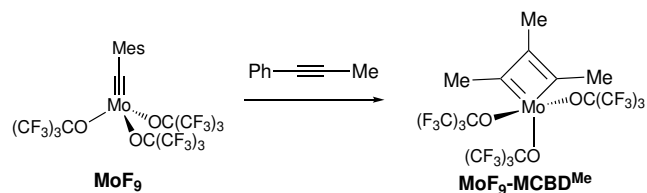
Figure 2. Self-metathesis of 1-phenyl-1-propyne catalyzed by MoF_9 (5.7×10^{-5} M) at various substrate concentrations: 0.6 M (black), 0.36 M (green), 0.24 M (red), and 0.12 M (blue).

Trapping of Reaction Intermediates on Supported and Molecular Systems

We also attempted to observe the reaction intermediates by solid-state NMR. The surface species catalysts were reacted with carbon-13 labeled diphenylacetylene, resulting in carbon-13 enrichment of the alkyldiene carbon. For $\text{MoF}_9/\text{SiO}_{2-700}$, $\text{MoF}_3/\text{SiO}_{2-700}$, and $\text{MoF}_6/\text{SiO}_{2-700}$ signals at isotropic chemical shifts of 284 ppm, 293 ppm, and 301 ppm, respectively, were observed by ^{13}C NMR after reaction with ^{13}C dilabeled diphenylacetylene, indicating the formation of ^{13}C labeled surface alkyldiene species. In contrast, applying the same procedure to $\text{MoF}_9/\text{SiO}_{2-700}$ revealed a signal at 313 ppm attributed to the surface Mo alkyldiene species, as well as two other signals at 253 ppm and 146 ppm. These additional peaks are consistent with the formation of a metallacyclobutadiene (MCBD) intermediate.^{63, 67-70}

Following the observation of the metallacyclobutadiene intermediates in the supported $\text{MoF}_9/\text{SiO}_{2-700}$ catalyst, these intermediates were also successfully trapped in the reaction of MoF_9 and 1-phenyl-1-propyne, which yields the corresponding methyl-substituted metallacyclobutadiene $\text{MoF}_9\text{-MCBD}^{\text{Me}}$ (Scheme 2).

Scheme 2. Synthesis of $\text{MoF}_9\text{-MCBD}^{\text{Me}}$ from molecular MoF_9 .



The isolation is possible by treating a saturated CH_2Cl_2 solution of MoF_9 with 10 equiv. of 1-phenyl-1-propyne. This reaction leads to an immediate color change from red to purple, an observation that is not made in the cases of MoF_0 , MoF_3 , and MoF_6 . Crystals of $\text{MoF}_9\text{-MCBD}^{\text{Me}}$ suitable for X-ray diffraction analysis form upon cooling the solution to $-40\text{ }^\circ\text{C}$. Unfortunately, the crystal structure exhibits a threefold modulation along the c -axis that cannot be sufficiently refined (see SI for more information). However, refinement with a non-modulated structure model is sufficient to determine the connectivity of $\text{MoF}_9\text{-MCBD}^{\text{Me}}$, which reveals a four-membered MoC_3 ring with a pentacoordinated molybdenum atom (Figure 3). The environment around the Mo atom can be described as distorted trigonal-bipyramidal with the atoms O1, C1 and C3 in equatorial and the atoms O2 and O2' in axial positions. Alternatively, a square-pyramidal geometry can be assigned with C3 in the apical position and with C1, O1, O2 and O2' forming the basal plane. Similar considerations have been made for structurally characterized tungstenacyclobutadienes of the type $[(\text{C}_3\text{R}_3)\text{WX}_3]$ (R = alkyl, aryl; X = alkoxide, phenoxide, amide, halide).^{46, 70-72} It should be noted that, to the best of our knowledge, $\text{MoF}_9\text{-MCBD}^{\text{Me}}$ represents the first structurally characterized metallacyclobutadiene of the type $[(\text{C}_3\text{R}_3)\text{MoX}_3]$, despite the isolation and spectroscopic characterization of such species.⁶⁷⁻⁶⁹ Additionally, solution NMR spectra showed the expected chemical shifts for $\text{MoF}_9\text{-MCBD}^{\text{Me}}$ with two low field signals in the ^{13}C NMR at 253 and 146 ppm for the α, α' (the two \square -carbon atoms cannot be distinguished in this case, vide infra) and β carbon atoms, respectively. The ^{19}F NMR spectrum shows two multiplets at -72.5 (9F) and -72.7 ppm (18F).

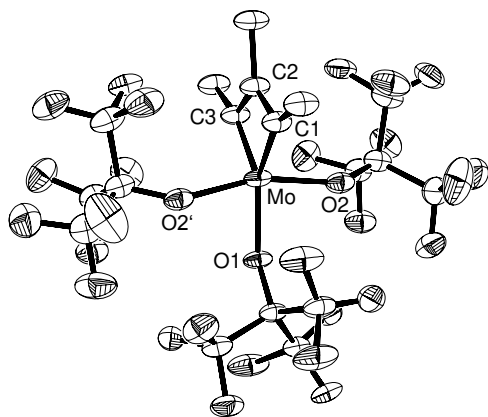


Figure 3. ORTEP diagram of **MoF₉-MCBD^{Me}** with thermal displacement parameters drawn at 50% probability. The molecule is located on a mirror plane. Hydrogen atoms and disordered OC(CF₃)₃ groups are omitted for clarity.

Linking NMR parameters and electronic properties.

We analyzed the observed isotropic chemical shifts and associated chemical shift tensors (CST) of the alkylidyne carbons, in view of the empirical correlation between the chemical shift, the σ -donation of the ligands and the reactivity of these catalysts. Since ¹³C chemical shifts are governed, like reactivity, by frontier molecular orbitals, analysis of the relevant NMR features can give valuable insights into the electronic structure of molecules⁷³ and dynamics.⁷⁴ In fact, we have recently exploited this approach to understand the relationship between the structure and the reactivity of alkylidenes and metallacyclobutanes, the two key olefin metathesis intermediates.⁷⁵⁻⁷⁷

In particular, the CST can be readily measured by ¹³C MAS NMR spectroscopy at low spinning rate and calculated by DFT methods.⁷⁸⁻⁷⁹ An orbital analysis, closely related to the original Natural Chemical Shift (NCS) analysis,⁸⁰⁻⁸² of the computed shielding provides detailed insight into the nature of the frontier orbitals, helping to relate the electronic structure of reaction intermediates with activity.⁸³⁻¹⁰²

Applying this approach to alkyne metathesis catalysts, the chemical shift tensor components ($\delta_{11} > \delta_{22} > \delta_{33}$) of the alkylidyne carbon signals are first collected by measuring the ¹³C{¹H} CP MAS NMR of the molecular alkylidynes **MoF_n** (n = 0, 3, 6, and 9) as well as **MoF₆-TBOS** and **Mo(TBOS)₃**, an additional

model compound with three tris(*tert*-butoxy)siloxy ligands, at low spinning rates (Table 4). All alkylidyne show highly anisotropic signals that are axially symmetric. The δ_{11} and δ_{22} tensor components are highly deshielded (up to 500 ppm) while the third component is remarkably shielded (around -15 ppm). As the electron withdrawing character of the alkoxide ligand increases, δ_{11} and δ_{22} become more deshielded, while δ_{33} remains relatively constant, leading overall to a more deshielded δ_{iso} . The same data are obtained for the surface-supported alkylidyne (^{13}C labeled on the alkylidyne position), which show similar highly anisotropic and axially symmetric chemical shift tensors. As compared to their molecular precursors, the δ_{11} and δ_{22} values of the surface species are consistently 10–30 ppm lower than those of the molecular complex (*vide infra*), leading to a significantly lower δ_{iso} . We also recorded the CSA of the metallacyclobutadiene intermediate formed by reaction of $\text{MoF}_9/\text{SiO}_{2-700}$ with diphenylacetylene, $\text{MoF}_9/\text{SiO}_{2-700}\text{-MCBD}$, as well as the molecular analogue obtained in the reaction of MoF_9 with 1-phenyl-1-propyne, $\text{MoF}_9\text{-MCBD}^{\text{Me}}$. These compounds display remarkably deshielded α/α' -(>250 ppm) and β -carbons (ca. 150 ppm) associated with remarkably large spans ($\Omega = \delta_{11} - \delta_{33}$).

Table 4. Measured chemical shift tensor principal components of molecular and surface alkylidyne species, as well as of α - and β -carbon atoms of MoF_9 -based metallacyclobutadiene intermediates.

Compound	δ_{iso}	δ_{11}	δ_{22}	δ_{33}
MoF_0	296	453	451	-15
MoF_3	308	471	468	-14
MoF_6	317	487	479	-15
$\text{MoF}_6\text{-TBOS}$	306	472	471	-24
MoF_9	331	497	487	$+10$
$\text{Mo}(\text{TBOS})_3$	303	457	457	-4
$\text{MoF}_0/\text{SiO}_{2-700}$	284	427	427	-1
$\text{MoF}_3/\text{SiO}_{2-700}$	293	448	446	-17
$\text{MoF}_6/\text{SiO}_{2-700}^{\text{a}}$	301	460	460	-17
$\text{MoF}_9/\text{SiO}_{2-700}$	313	488	484	-32
$\text{MoF}_9/\text{SiO}_{2-700}\text{-MCBD } \alpha$	253	476	186	$+98$

MoF₉/SiO₂₋₇₀₀⁻ MCBD β	146	258	190	-11
MoF₉-MCBD^{Me} α	274	540	167	+114
MoF₉-MCBD^{Me} α'	268	525	169	+109
MoF₉-MCBD^{Me} β	155	304	132	+29

^a similar value obtained by grafting labeled alkyldiyne. C(□) and C(□') of MCBD are doubly and singly bonded to Mo, respectively.

Analysis of the NMR Chemical Shifts.

The shielding tensors of the alkyldiyne **MoF_n** (n = 0, 3, 6, and 9), **MoF₆-TBOS** and **Mo(TBOS)₃** are calculated with two-component ZORA¹⁰³⁻¹⁰⁷ DFT calculations (PBE0¹⁰⁸/TZ2P) (see computational details in SI). The calculated isotropic chemical shifts of the molecular alkyldiyne **MoF_n** (Table 5) agree well with experimental data (Table 4) with a maximum deviation of less than 20 ppm, while the calculated and experimental principal components differ more, possibly due to the presence, at least in part, of dynamics (*vide infra*).

The shielding tensor σ (eq. 1) of an NMR active nucleus can be decomposed into diamagnetic and paramagnetic and spin-orbit (SO) terms (eq. 2). Both interactions are caused by electronic currents induced by the magnetic field. While the diamagnetic contribution, which originates from magnetic currents within orbitals in the ground state, is usually close to isotropic, the paramagnetic contribution completed by the spin-orbit coupling term reflects the anisotropic bonding of the atom. In the present study, the $\square_{\text{para+SO}}$ term is found to be dominated by the paramagnetic contribution, in line with previous reports on alkyldiyne systems⁷⁵ (Table S8). Thus, while the calculations include the spin-orbit coupling, the $\square_{\text{para+SO}}$ term will be interpreted solely based on the paramagnetic contribution, which is dominated by the magnetically induced coupling of occupied (*occ*) and vacant (*vac*) frontier orbitals of appropriate symmetry (eq. 3) as already shown for the alkyldiyne and metallacyclobutanes.⁷⁵⁻⁷⁷

$$\begin{pmatrix} \delta_{11} & 0 & 0 \\ 0 & \delta_{22} & 0 \\ 0 & 0 & \delta_{33} \end{pmatrix} = \sigma_{\text{iso}}^{\text{ref}} \begin{pmatrix} 1 & 0 & 0 \\ 0 & 1 & 0 \\ 0 & 0 & 1 \end{pmatrix} - \begin{pmatrix} \sigma_{11} & 0 & 0 \\ 0 & \sigma_{22} & 0 \\ 0 & 0 & \sigma_{33} \end{pmatrix} \quad (1)$$

$$\sigma = \sigma_{dia} + \sigma_{para+so} \quad (2)$$

$$\sigma_{ii,para} \propto \frac{\langle \Psi_{vac} | \hat{L}_i | \Psi_{occ} \rangle \langle \Psi_{vac} | \hat{L}_i / r^3 | \Psi_{occ} \rangle}{\Delta E_{vac-occ}} \quad (3)$$

Table 5. Calculated ^{13}C NMR chemical shifts (shielding in parenthesis) and principal tensor components of the alkylidynes.

Compound	δ_{iso} (σ_{iso})	δ_{11} (σ_{11})	δ_{22} (σ_{22})	δ_{33} (σ_{33})
MoF₀	314 (-123)	477 (-287)	444 (-254)	20 (171)
MoF₃	323 (-132)	495 (-304)	457 (-267)	16 (175)
MoF₆	333 (-143)	502 (-312)	478 (-288)	19 (172)
MoF₉	348 (-158)	536 (-346)	492 (-302)	16 (174)
MoF₆-TBOS	325 (-135)	485 (-295)	479 (-289)	10 (180)
Mo(TBOS)₃	318 (-127)	478 (-288)	445 (-254)	30 (160)

As found experimentally and computationally, the differences in isotropic chemical shift between the various alkylidynes are dominated by δ_{11} and δ_{22} . The calculations show that these two principal components are oriented perpendicularly to the M–C–Mes axis and are highly deshielded, while δ_{33} oriented along this axis is very shielded (Figure 4A), similarly to what is found for alkynes (Figure 4B).⁸⁶ However, contrary to experimental values of the tensor components, the calculated δ_{11} and δ_{22} differ significantly, which originates from the lack of a C_3 symmetry both in the solid state (X-ray) and calculated optimized structures. This is due to the presence of the aryl substituent on the alkylidyne group and the slight difference in the C–Mo–O angles for the three OR ligands with a more acute value for one of them. Presumably, an average C_3 axis is established on the NMR timescale by fast rotation around the

C^{sp}-aryl bond and an equilibration of the C-Mo-O angles even at 100 K, resulting in equal δ_{11} and δ_{22} . In the non-averaged optimized structures, the most deshielded component (δ_{11}) is oriented perpendicularly to the plane of the aromatic moiety, while δ_{22} lies in the same plane (Figures 4A and 4B).

The values of the diamagnetic and paramagnetic contributions calculated for diphenylacetylene and **MoF_n** ($n = 0, 3, 6,$ and 9) as well as **MoF₆-TBOS** showed that the diamagnetic contribution is similar in all compounds (Figure S33). Notably however, the diamagnetic contribution to δ_{33}/σ_{33} is generally higher than for the two other principal components as previously shown for triply bonded carbon due to the presence of a C_∞ axis along the M \equiv C bond.⁸⁶ Nevertheless, the main differences in shielding between the various compounds mainly result from the paramagnetic contribution, which is larger in magnitude for δ_{11} and δ_{22} (Figure S33). In order to elucidate the origin of the variation of this term, an orbital analysis (related to the NCS analysis as mentioned previously, referred to as NCS in the following) is carried out to determine the individual orbital contributions. This analysis gives the contributions of the individual occupied NLMOs (Natural Localized Molecular Orbitals, *i.e.* bonds and lone pairs) to shielding, and hence establishes a direct link to the electronic structure of the chemical species.

For **MoF_n**, the NCS analysis shows that the observed deshielding for δ_{11} mainly results from the alkylidyne $\sigma(M\equiv C)$ bond, and to a lesser extent from the alkylidyne $\sigma(C-C_{Mes})$ bond (Figure 4C and Figure 4D for the specific example of **MoF₆**, other **MoF_n** see Figure S34). These orbitals are coupled to the vacant M \equiv C alkylidyne $\sigma^*(M\equiv C)$ orbital by action of the angular momentum operator perpendicular to the C_∞ axis and normal to the plane of the aromatic substituent. A smaller contribution also arises from the coupling of the $\pi(M\equiv C)$ orbital to the $\sigma^*(M\equiv C)$ orbital. A similar picture is found for δ_{22} when considering the corresponding angular momentum operator which is perpendicular to the M \equiv C axis and in the plane of the aromatic substituent (Figure S35).

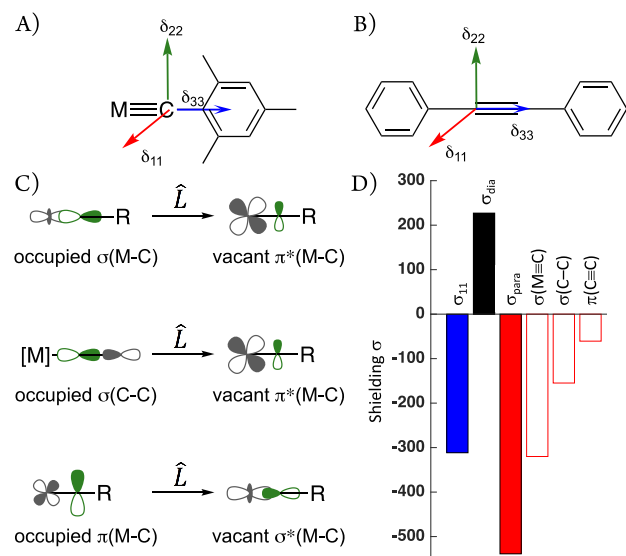


Figure 4. Orientation of the calculated shielding tensors of (A) MoF_n and (B) diphenylacetylene. (C) Relevant orbital couplings giving rise to deshielding of δ_{11} in MoF_n . D) NCS analysis of σ_{11} of alkyldiyne carbon for MoF_6 (see Figure S34 for other MoF_n).

Figures S34 and S35 show that the deshielding of δ_{11} and δ_{22} increase in the series MoF_0 – MoF_3 – MoF_6 – MoF_9 . Since the paramagnetic term increases with a decreasing energy gap between the coupled $\sigma(\text{M}\equiv\text{C})$ and $\sigma(\text{C}-\text{C}_{\text{Mes}})$ occupied and empty $\pi^*\text{M}\equiv\text{C})$ orbitals (eq. 3), this analysis indicates that the energy of the $\pi^*(\text{M}\equiv\text{C})$ orbitals are lowered as more fluorine atoms are introduced onto the alkoxy ligands.

Noteworthy, replacing one OtBuF_6 ligand in MoF_6 by a tris-*tert*-butoxy-siloxy ligand (TBOS) or considering $\text{Mo}(\text{TBOS})_3$, gives NMR features that are similar to MoF_3 . These data suggest that the electronic properties of the *tert*-butoxy-siloxy ligand are similar to OtBuF_3 . Analogous results were previously found for W-metallacyclobutanes, albeit placing the tris-*tert*-butoxy-siloxy ligand in between OtBuF_3 and OtBuF_6 .¹⁰⁹⁻¹¹⁰

For the most shielded component δ_{33} , the NCS analysis shows only minor paramagnetic contributions for all investigated alkyldynes. This is expected due to the pseudo C_∞ -symmetry, which leads to vanishing paramagnetic contributions along the C_∞ -axis as found in alkynes (Figure S33 and S36).⁸⁶

The conclusion drawn from the NCS analysis (*i.e.* that electron withdrawing ligands lower the energy of the $\pi^*(M\equiv C)$ orbitals) is in line with the observation that alkylidyne catalysts with the most deshielded tensor components δ_{11} and δ_{22} tend to be the most efficient catalysts for alkyne metathesis. A lower $\pi^*(M\equiv C)$ orbital should lead to more facile alkyne coordination as the substrate plays the role of donor in its interaction with the catalyst, the only exception being **MoF₉**, which shows low activity due to the formation of a stable metallacyclobutadiene intermediate, consistent with the 0th order dependence of the reaction in the alkyne substrate and its observation under reaction conditions of alkyne metathesis.

NMR shieldings and the associated NCS analysis in metallacyclobutadienes.

Kinetic studies and NMR measurements of the intermediates show the formation of a stable metallacyclobutadiene with **MoF₉**, which is thus a resting state of the catalyst. Similarly, a metallacyclobutadiene is also detected for the corresponding silica-supported systems. The chemical shift tensors of these compounds, measured by solid-state NMR, are shown in Table 4.

In order to complement these observations, DFT calculations of the intermediates are carried out for the reaction of diphenylacetylene with the molecular catalysts **MoF₀**, **MoF₃**, **MoF₆**, and **MoF₉** (PBE0¹⁰⁸/pcSseg-2¹¹¹; SDD ECP¹¹²⁻¹¹⁴ on Mo, GD3 dispersion¹¹⁵; solvent (toluene) effect with the SMD method¹¹⁶, see Supporting Information for full details). This model reaction was chosen for the computational analysis because it gives rise to symmetrically phenyl-substituted metallacyclobutadienes, which have been experimentally observed for **MoF₉/SiO₂₋₇₀₀**. The metallacyclobutadiene becomes increasingly stable relative to separated diphenylacetylene and alkylidyne catalyst as the number of fluorine atoms increases on the alkoxy ligands. ΔG_{298} values for the reaction of alkylidyne and diphenylacetylene to the metallacyclobutadiene are 11.0, 6.6, 2.6, and -0.9 kcal/mol for **MoF₀**, **MoF₃**, **MoF₆**, and **MoF₉**, respectively. For **MoF₉**, ΔG_{298} is negative, in agreement with the observation of the corresponding metallacyclobutadiene. Thus, both the experiments and calculations suggest that the metallacyclobutadiene of **MoF₉** is a resting state of the catalyst, which is consistent with the decrease in activity and the change of reaction order upon going from **MoF₆** to **MoF₉**. A similar trend is also found for

the reaction of 2-butyne with the corresponding ethylidyne catalysts, where the calculated ΔG_{298} values for the formation of the methyl substituted metallacyclobutadienes are 9.8, 0.6, -1.5, and -9.1 kcal/mol for the ethylidyne derivatives of **MoF₀**, **MoF₃**, **MoF₆**, and **MoF₉**, respectively.

To gain insight in the NMR properties of the metallacyclobutadienes, the shielding tensors are calculated and analyzed for the metallacyclobutadienes resulting from a reaction of **MoF₀**, **MoF₃**, **MoF₆**, and **MoF₉** with diphenylacetylene as a model reaction for both molecular and supported catalysts. We also calculate the methyl-substituted analogue **MoF₉-MCBD^{Me}** to further benchmark the NMR calculations by comparison to an isolated molecular system. For this compound, good agreement is found between the isotropic calculated and experimental chemical shifts as well as the principal components of the CST (Table 6 and Table S6).

Table 6. Calculated chemical shifts and principal components of **MoF₉-MCBD^{Me}** (see Table 4 for measured values). C(α) and C(α') are doubly and singly bonded to Mo, respectively (see Table S6 for other metallacyclobutadienes).

nucleus	δ_{iso} (σ_{iso})	δ_{11} (σ_{11})	δ_{22} (σ_{22})	δ_{33} (σ_{33})
C(α)	276 (-86)	556 (-366)	179 (12)	94 (97)
C(α')	267 (-77)	530 (-339)	146 (45)	126 (64)
C(β)	157 (33)	322 (-132)	233 (-42)	-83 (273)

In the metallacyclobutadiene formed upon [2+2] cycloaddition of the alkyne to the alkylidyne, the α -carbon atom doubly bonded to the metal, C(α), originates from the alkylidyne carbon, while the carbons connected by a double bond (labeled as C(α') and C(β)) originate from the alkyne. Notably, the C(α) and

C(α') carbon atoms of the metallacyclobutadiene show distinct chemical shift tensors, underlining that the metallacyclobutadiene can exist as two regioisomers.

For C(α), the most deshielded component of the CST (δ_{11}/σ_{11}) is oriented along the C(α)-C(β)-bond, while the most shielded component (δ_{33}/σ_{33}) is oriented along the M-C(α) axis (Figure 5 and S38). As compared to the parent alkylidyne, the δ_{11} component remains rather unaffected by the metallacyclobutadiene formation, while the δ_{22} component becomes significantly more shielded, evidencing the smaller contribution of the corresponding alkylidyne $\pi^*(M\equiv C)$ orbital, which is involved into bonding in the plane of the ring, leading to disappearance of one alkylidyne π -bond.

For C(α'), the most deshielded component (δ_{11}/σ_{11}) is oriented along the C(α')-C(β) bond as found for C(α). The orientation of the other two components depends on the nature of the alkoxide (Figure S39). While the most shielded component (δ_{33}/σ_{33}) is oriented perpendicularly to the ring in **MoF₀-MCBD**, **MoF₃-MCBD**, and **MoF₆-MCBD**, it is oriented along the M-C(α') axis in **MoF₉-MCBD**. In other words, the tensors on C(α') and C(α) become more similar with increasing fluorination of the alkoxide ligands, which parallels the more symmetrical structure of the metallacyclobutadiene (similar M-C(α/α') and C(α/α')-C(β) bond lengths, see Table S5). The more symmetrical cyclic structure for **MoF₉-MCBD** is also in line with a thermodynamically more favorable metallacyclobutadiene formation, as observed both experimentally and computationally (a more symmetric metallacyclobutadiene is closer to the transition state of metallacyclobutadiene interconversion than to the transition state of cycloreversion).

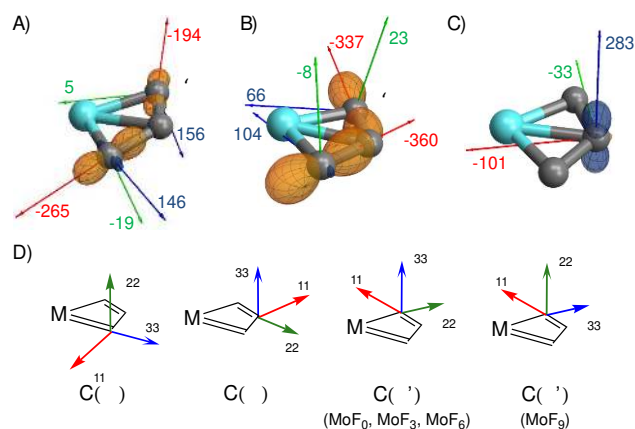


Figure 5. Calculated shielding tensors of the α -carbon atoms in **MoF₀-MCBD** (A) and **MoF₉-MCBD** (B), and the β -carbon in **MoF₉-MCBD** (C). All ligands and substituents have been removed for clarity. The carbon originating from the alkyidyne is shown in the front. D) Schematic representation of orientation of shielding tensors in metallacyclobutadienes derived from **MoF₀**, **MoF₃**, **MoF₆** and **MoF₉**.

The NCS analysis shows that the deshielding in the plane of the metallacyclobutadiene arises from the couplings of M–C and C–C σ orbitals (the bonds in the plane of the ring) with the antibonding orbitals of the metallacyclobutadiene π -system. Increasing fluorination leads to larger deshielding, evidencing a lower lying π^* system in the metallacyclobutadienes with more electron withdrawing substituents. This orbital is probably involved in the stabilization of these intermediates and participates in the electron redistribution during the interconversion between the two metallacyclobutadiene isomers.

Discussions

We have observed that the chemical shift of the alkyidyne carbon atom becomes more deshielded with increasing electron withdrawing character of the alkoxide ligand (**MoF₀** < **MoF₃** < **MoF₆** < **MoF₉**). The alkyidyne chemical shift of the molecular siloxide derivative (**MoF₆-TBOS**) or **Mo(TBOS)₃** also falls close to that of **MoF₃**, consistent with the similar electronic characters of *Ot*BuF₃ and the siloxy group, OSi(*Ot*Bu)₃. This is in line with the previous observation of the TBP/SP ratio in d⁰ metallacyclobutane intermediates, albeit placing OSi(*Ot*Bu)₃ in between *Ot*BuF₃ and *Ot*BuF₆.¹⁰⁹⁻¹¹⁰ NCS analysis shows that the alkyidyne chemical shift directly probes the energy of $\pi^*(M\equiv C)$, the more deshielded, the lower the

$\pi^*(M\equiv C)$ and in principle the higher the reactivity. In fact, this translates into an increase of alkyne metathesis activity from **MoF₀**, **MoF₃** up to **MoF₆** before sharply decreasing for **MoF₉** (volcano plot of reactivity: **MoF₆** > **MoF₃** > **MoF₀** > **MoF₉**). This decrease in activity is also associated with a different kinetic behavior. This is due to the formation a significantly more stable metallacyclobutadiene intermediate, which is isolated and fully characterized by X-ray crystallography (in the case of **MoF₉-MCBD^{Me}**) and solid-state NMR. According to calculations, the **MoF₉** metallacyclobutadiene is in fact more stable than the separated reactants and displays a much more symmetric ring with similar Mo–C(α/α') and C(α/α')–C(β) distances, further illustrating that it lies further away from the isolated alkylidyne and alkyne reactants. The increased stabilization of the **MoF₉** metallacyclobutadiene leads to a change of the rate-determining step, from metallacyclobutadiene formation to cycloreversion. This means that further stabilization of the metallacyclobutadiene intermediate (as caused by increasing the electron withdrawing nature of the alkoxide ligands) will in fact *raise* the reaction barrier and thereby decrease the rate of metathesis.

The corresponding silica-supported analogues are much less active in the self-metathesis of 1-phenyl-1-propyne and show a similar volcano reactivity plot, albeit with a different order of reactivity (**MoF₃/SiO₂₋₇₀₀** > **MoF₆/SiO₂₋₇₀₀** > **MoF₀/SiO₂₋₇₀₀** > **MoF₉/SiO₂₋₇₀₀**). In addition, the silica-supported compounds display a much more shielded alkylidyne carbon by comparison with the respective molecular precursors, by ca. 10-20 ppm. This increased shielding mainly results from the significantly more shielded δ_{11} and δ_{22} components of the chemical shift tensors, indicating a higher $\pi^*(M\equiv C)$, consistent with their overall lower activity. While for **MoF₃**, **MoF₆** and **MoF₉** the observed trend of an increase in shielding upon grafting can be reproduced by DFT/ZORA calculations, using (Me₃SiO)₃Si–OH as a model for the surface, this is not the case for **MoF₀**, in line with silanolate being a much weaker donor than *tert*-butanolate. The experimentally observed shielding of **MoF₀/SiO₂₋₇₀₀** can only be reproduced by calculations when introducing a secondary interaction of a surface OH-group with the 2,4,6-trimethylbenzylidyne moiety using a larger silica model (see Table S9). However, this interaction has little effect on chemical shift for the other complexes. The presence of such an interaction in supported catalysts is indeed in line with the

presence of red-shifted OH groups in the IR spectra (indicated with small red arrows in Figure S10), typical of silanol groups interacting with aromatics.⁶⁴

MoF₆-TBOS is also shielded as compared to **MoF₆**, albeit to a lesser extent than the surface supported analogue. In this compound, the shielding is mainly caused by the close contact to oxygen in the 2nd coordination sphere (as seen by DFT calculations with varying Mo–O distances, see Table S7). Such an interaction is absent in the supported catalyst according to EXAFS, suggesting that the observed shielding in the supported catalyst probably originates from the siloxy ligand and the presence of secondary interactions between the organometallic fragment and the silica surface. It is also consistent with the absence of dynamics at room temperature according to solid-state NMR, which shows that the metal fragment strongly interacts with the silica surface.⁷⁴ Overall, such an interaction is likely responsible for the observed decrease in activity upon grafting, due to both decreased dynamics of the surface species and the resulting lower electrophilicity of the metal center (high lying π^*).

Conclusion

Molecular and silica-supported Mo alkylidyne complexes display characteristic carbon chemical shifts and activities as a function of the number of fluorine atoms attached to the pendant alkoxide ligands. First, the chemical shift value of the alkylidyne carbon systematically increases with the increased number of fluorine atoms, which is rationalized by a decrease of the energy of the $\pi^*(M\equiv C)$ according to NCS analysis of the most deshielded chemical shift tensor principal components (δ_{11} and δ_{22}), measured experimentally and computed by two-component relativistic DFT/ZORA calculations. In addition, this analysis allows to classify the $(t\text{BuO})_3\text{SiO}$ ligand as having similar electronic properties as a $t\text{BuF}_3\text{O}$ group. More surprisingly perhaps, the silica-supported species show significantly more shielded values than the corresponding molecular complexes, suggesting that they are less electrophilic. Regarding metathesis performance, the activity in terms of turnover frequency goes through a maximum as a function of the number of fluorine atoms on the *tert*-butoxide ligand, namely three ($t\text{BuF}_3\text{O}$) and six ($t\text{BuF}_6\text{O}$) fluorine atoms for the silica-supported and homogeneous catalysts, respectively; the non-

fluorinated and the perfluorinated ligand yielding very low activity and overall catalyst performance (turnover number). This volcano-type behavior can be explained by the increased electrophilicity of the Mo sites (as shown by their NMR chemical shift) with increasing number of fluorine atoms, until an overly stable metallacyclobutadiene intermediate is formed. This is demonstrated by the characterization of metallacyclobutadiene intermediates for both **MoF₉**, molecular and supported catalysts and their associated kinetic behavior (0th order in substrate). As also suggested from the chemical shift, silica-supported alkyne metathesis catalysts are found less active, which is consistent with the decreased electrophilicity of the active sites as suggested by their NMR chemical shift. In addition, the absence of dynamics for the silica-supported systems in the solid-state NMR measurements probably also contributes to the lower activity (rates) of silica-supported catalysts. This study further illustrates the power of NMR spectroscopy in providing detailed information about electronic structures and dynamics, which are two important factors driving catalyst performance.¹¹⁷ We are currently further exploring this field of research with the goal to develop efficient descriptors to predict reactivity of metal sites.

ACKNOWLEDGMENT

The authors are grateful to the Scientific Equipment Program of ETH Zürich and the SNSF (R'Equip grant 206021_150709/1) for financial support of the high throughput catalyst screening facility (HTE@ETH). D.P.E. was supported by an ETH Postdoctoral Fellowship (jointly funded by ETH Zürich and Marie Curie Action for People, FEL-16 14-2). The work of C.P.G and W.C.L is supported by SNF grant number 200021_169134 and 200020_149704, respectively. A.F. thanks Holcim Stiftung for a habilitation fellowship. Funding by the Deutsche Forschungsgemeinschaft (DFG) through project Ta 189/12-1 ("Mechanistic studies on the catalytic metathesis of internal and terminal alkynes and diynes") is also acknowledged. H.E. is grateful to the Fonds der Chemischen Industrie (FCI) for a Chemiefonds Fellowship. We also want to thank O. V. Safonova for EXAFS measurements and discussions as well as Òscar Àrias for providing ¹³C-labeled diphenylacetylene.

REFERENCES

- (1) Fürstner, A. *Angew. Chem. Int. Ed.* **2000**, *39*, 3012-3043.
- (2) Hoveyda, A. H.; Zhugralin, A. R. *Nature.* **2007**, *450*, 243-251.
- (3) Grubbs, R. H., *Handbook of Metathesis*. Wiley-VCH: Weinheim, Germany, 2014; Vol. 1-3.
- (4) Grela, K., *Olefin Metathesis: Theory and Practice*. Wiley VCH: Weinheim, 2014.
- (5) Higman, C. S.; Lummiss, J. A. M.; Fogg, D. E. *Angew. Chem. Int. Ed.* **2016**, *55*, 3552-3565.
- (6) Fürstner, A.; Davies, P. W. *Chem. Commun.* **2005**, 2307-2320.
- (7) Coutelier, O.; Mortreux, A. *Adv. Synth. Catal.* **2006**, *348*, 2038–2042.
- (8) Cho, H. M.; Weissman, H.; Wilson, S. R.; Moore, J. S. *J. Am. Chem. Soc.* **2006**, *128*, 14742-14743.
- (9) Schrock, R. R.; Czekelius, C. *Adv. Synth. Catal.* **2007**, *349*, 55-77.
- (10) Zhang, W.; Moore, J. S. *Adv. Synth. Catal.* **2007**, *349*, 93-120.
- (11) Wu, X.; Tamm, M. *Beilstein J. Org. Chem.* **2011**, *7*, 82-93.
- (12) Jyothish, K.; Zhang, W. *Angew. Chem. Int. Ed.* **2011**, *50*, 8478–8480.
- (13) Fürstner, A. *Angew. Chem. Int. Ed.* **2013**, *52*, 2794–2819.
- (14) Schrock, R. R. *Acc. Chem. Res.* **1986**, *19*, 342–348.
- (15) Schrock, R. R. *Chem. Rev.* **2001**, *102*, 145-180.
- (16) Schrock, R. R. *Chem. Commun.* **2013**, *49*, 5529–5531.
- (17) Beer, S.; Hrib, C. G.; Jones, P. G.; Brandhorst, K.; Grunenberg, J.; Tamm, M. *Angew. Chem. Int. Ed.* **2007**, *46*, 8890–8894.

- (18) Fischer, F. R.; Nuckolls, C. *Angew. Chem. Int. Ed.* **2010**, *49*, 7257–7260.
- (19) Haberlag, B.; Freytag, M.; Daniliuc, C. G.; Jones, P. G.; Tamm, M. *Angew. Chem. Int. Ed.* **2012**, *51*, 13019–13022.
- (20) Haberlag, B.; Freytag, M.; Jones, P. G.; Tamm, M. *Adv. Synth. Catal.* **2014**, *356*, 1255–1265.
- (21) von Kugelgen, S.; Sifri, R.; Bellone, D.; Fischer, F. R. *J. Am. Chem. Soc.* **2017**, *139*, 7577–7585.
- (22) Koy, M.; Elser, I.; Meisner, J.; Frey, W.; Wurst, K.; Kaestenr, J.; Buchmeiser, M. R. *Chem. Eur. J.* doi: 10.1002/chem.201703313.
- (23) Jyothish, K.; Wang, Q.; Zhang, W. *Adv. Synth. Catal.* **2012**, *354*, 2073–2078.
- (24) Sedbrook, D. F.; Paley, D. W.; Steigerwald, M. L.; Nuckolls, C.; Fischer, F. R. *Macromolecules* **2012**, *45*, 5040–5044.
- (25) Du, Y.; Yang, H.; Zhu, C.; Ortiz, M.; Okochi, K. D.; Shoemaker, R.; Jin, Y.; Zhang, W. *Chem. Eur. J.* **2016**, *22*, 7959–7963.
- (26) Heppekausen, J.; Stade, R.; Goddard, R.; Fürstner, A. *J. Am. Chem. Soc.* **2010**, *132*, 11045–11057.
- (27) Lysenko, S.; Haberlag, B.; Daniliuc, C. G.; Jones, P. G.; Tamm, M. *ChemCatChem* **2011**, *3*, 115–118.
- (28) Heppekausen, J.; Stade, R.; Kondoh, A.; Seidel, G.; Goddard, R.; Fürstner, A. *Chem. Eur. J.* **2012**, *18*, 10281–10299.
- (29) Lysenko, S.; Volbeda, J.; Jones, P. G.; Tamm, M. *Angew. Chem. Int. Ed.* **2012**, *51*, 6757–6761.
- (30) Li, S. T.; Schnabel, T.; Lysenko, S.; Brandhorst, K.; Tamm, M. *Chem. Commun.* **2013**, *49*, 7189–7191.

- (31) Beer, S.; Brandhorst, K.; Hrib, C. G.; Wu, X.; Haberlag, B.; Grunenberg, J.; Jones, P. G.; Tamm, M. *Organometallics* **2009**, *28*, 1534-1545.
- (32) Haberlag, B.; Wu, X.; Brandhorst, K.; Grunenberg, J.; Daniliuc, C. G.; Jones, P. G.; Tamm, M. *Chem. Eur. J.* **2010**, *16*, 8868–8877.
- (33) Yang, H.; Jin, Y.; Du, Y.; Zhang, W. *J. Mater. Chem. A* **2014**, *2*, 5986–5993.
- (34) Bellone, D. E.; Bours, J.; Menke, E. H.; Fischer, F. R. *J. Am. Chem. Soc.* **2015**, *137*, 850–856.
- (35) von Kugelgen, S. W.; Bellone, D. E.; Cloke, R. R.; Perkins, W. S.; Fischer, F. R. *J. Am. Chem. Soc.* **2016**, *138*, 6234-6239.
- (36) Persich, P.; Llaveria, J.; Lhermet, R.; de Haro, T.; Stade, R.; Kondoh, A.; Fürstner, A. *Chem. Eur. J.* **2013**, *19*, 13047–13058.
- (37) Valot, G.; Mailhol, D.; Regens, C. S.; O'Malley, D. P.; Godineau, E.; Takikawa, H.; Philipps, P.; Fürstner, A. *Chem. Eur. J.* **2015**, *21*, 2398–2408.
- (38) Willwacher, J.; Heggen, B.; Wirtz, C.; Thiel, W.; Fürstner, A. *Chem. Eur. J.* **2015**, *21*, 10416-10430.
- (39) Ungeheuer, F.; Fürstner, A. *Chem. Eur. J.* **2015**, *21*, 11387-11392.
- (40) Cromm, P. M.; Schaubach, S.; Spiegel, J.; Fürstner, A.; Grossmann, T. N.; Waldmann, H. *Nat. Commun.* **2016**, *7*, 11300.
- (41) Cromm, P. M.; Wallraven, K.; Glas, A.; Bier, D.; Fürstner, A.; Ottmann, C.; Grossmann, T. N. *ChemBioChem* **2016**, *17*, 1915-1919.
- (42) Ahlers, A.; de Haro, T.; Gabor, B.; Fürstner, A. *Angew. Chem. Int. Ed.* **2016**, *55*, 1406-1411.
- (43) Schaubach, S.; Michigami, K.; Fürstner, A. *Synthesis* **2017**, *49*, 202-208.
- (44) Strutz, H.; Schrock, R. R. *Organometallics* **1984**, *3*, 1600-1601.

- (45) Schrock, R. R.; Pedersen, S. F.; Churchill, M. R.; Ziller, J. W. *Organometallics* **1984**, *3*, 1574-1583.
- (46) Churchill, M. R.; Ziller, J. W.; Freudenberger, J. H.; Schrock, R. R. *Organometallics* **1984**, *3*, 1554-1562.
- (47) Lin, Z.; Hall, M. B. *Organometallics* **1994**, *13*, 2878-2884.
- (48) Blanc, F.; Copéret, C.; Thivolle-Cazat, J.; Basset, J.-M.; Lesage, A.; Emsley, L.; Sinha, A.; Schrock, R. R. *Angew. Chem. Int. Ed.* **2006**, *45*, 1216-1220.
- (49) Rascon, F.; Wischert, R.; Copéret, C. *Chem. Sci.* **2011**, *2*, 1449-1456.
- (50) Chabanas, M.; Baudouin, A.; Copéret, C.; Basset, J.-M. *J. Am. Chem. Soc.* **2001**, *123*, 2062-2063.
- (51) Copéret, C.; Comas-Vives, A.; Conley, M. P.; Estes, D. P.; Fedorov, A.; Mougél, V.; Nagae, H.; Núñez-Zarur, F.; Zhizhko, P. A. *Chem. Rev.* **2016**, *116*, 323-421.
- (52) Copéret, C.; Allouche, F.; Chang, K. W.; Conley, M.; Delley, M. F.; Fedorov, A.; Moroz, I.; Mougél, V.; Pucino, M.; Searles, K.; Yamamoto, K.; Zhizhko, P. *Angew. Chem. Int. Ed.*, doi: 10.1002/anie.201702387.
- (53) Petroff Saint-Arroman, R.; Chabanas, M.; Baudouin, A.; Copéret, C.; Basset, J.-M.; Lesage, A.; Emsley, L. *J. Am. Chem. Soc.* **2001**, *123*, 3820-3821.
- (54) Weissman, H.; Plunkett, K. N.; Moore, J. S. *Angew. Chem. Int. Ed.* **2006**, *45*, 585-588.
- (55) Cho, H. M.; Weissman, H.; Moore, J. S. *J. Org. Chem.* **2008**, *73*, 4256-4258.
- (56) Merle, N.; Taoufik, M.; Nayer, M.; Baudouin, A.; Roux, E. L.; Gauvin, R. M.; Lefebvre, F.; Thivolle-Cazat, J.; Basset, J.-M. *J. Organomet. Chem.* **2008**, *693*, 1733-1737.
- (57) Genelot, M.; Cheval, N. P.; Vitorino, M.; Berrier, E.; Weibel, J.-M.; Pale, P.; Mortreux, A.; Gauvin, R. M. *Chem. Sci.* **2013**, *4*, 2680-2685.

- (58) Estes, D. P.; Bittner, C.; Àrias, Ò.; Casey, M.; Fedorov, A.; Tamm, M.; Copéret, C. *Angew. Chem. Int. Ed.* **2016**, *55*, 13960-13964.
- (59) Hock, A. S.; Schrock, R. R.; Hoveyda, A. H. *J. Am. Chem. Soc.* **2006**, *128*, 16373-16375.
- (60) Pucino, M.; Mougél, V.; Schowner, R.; Fedorov, A.; Buchmeiser, M. R.; Copéret, C. *Angew. Chem. Int. Ed.* **2016**, *55*, 4300-4302.
- (61) Koh, M. J.; Nguyen, T. T.; Lam, J. K.; Torker, S.; Hyvl, J.; Schrock, R. R.; Hoveyda, A. H. *Nature* **2017**, *542*, 80-85.
- (62) Carpentier, J.-F. *Dalton Trans.* **2010**, *39*, 37-48.
- (63) Bittner, C.; Ehrhorn, H.; Bockfeld, D.; Brandhorst, K.; Tamm, M. *Organometallics* **2017**, *36*, 3398-3406.
- (64) Rhers, B.; Salameh, A.; Baudouin, A.; Quadrelli, E. A.; Taoufik, M.; Copéret, C.; Lefebvre, F.; Basset, J.-M.; Solans-Monfort, X.; Eisenstein, O.; Lukens, W. W.; Lopez, L. P. H.; Sinha, A.; Schrock, R. *Organometallics* **2006**, *25*, 3554-3557.
- (65) Lataste, E.; Legein, C.; Body, M.; Buzaré, J.-Y.; Tressaud, A.; Demourgues, A. *J. Phys. Chem. C* **2009**, *113*, 18652-18660.
- (66) Demourgues, A.; Lataste, E.; Durand, E.; Tressaud, A., Access to Highly Fluorinated Silica by Direct F₂ Fluorination. In *Functionalized Inorganic Fluorides*, John Wiley & Sons, Ltd: 2010; pp 519-543.
- (67) McCullough, L. G.; Schrock, R. R. *J. Am. Chem. Soc.* **1984**, *106*, 4067-4068.
- (68) McCullough, L. G.; Schrock, R. R.; Dewan, J. C.; Murdzek, J. C. *J. Am. Chem. Soc.* **1985**, *107*, 5987-5998.
- (69) Schrock, R. R.; Jamieson, J. Y.; Araujo, J. P.; Bonitatebus Jr, P. J.; Sinha, A.; Lopez, L. P. H. *J. Organomet. Chem.* **2003**, *684*, 56-67.

- (70) O'Reilly, M. E.; Ghiviriga, I.; Abboud, K. A.; Veige, A. S. *Dalton Trans.* **2013**, 42, 3326-3336.
- (71) Pedersen, S. F.; Schrock, R. R.; Churchill, M. R.; Wasserman, H. J. *J. Am. Chem. Soc.* **1982**, 104, 6808-6809.
- (72) Freudenberger, J. H.; Schrock, R. R.; Churchill, M. R.; Rheingold, A. L.; Ziller, J. W. *Organometallics* **1984**, 3, 1563-1573.
- (73) Widdifield, C. M.; Schurko, R. W. *Concepts Magn Res Part A* **2009**, 34A, 91-123.
- (74) Blanc, F.; Basset, J.-M.; Copéret, C.; Sinha, A.; Tonzetich, Z. J.; Schrock, R. R.; Solans-Monfort, X.; Clot, E.; Eisenstein, O.; Lesage, A.; Emsley, L. *J. Am. Chem. Soc.* **2008**, 130, 5886-5900.
- (75) Halbert, S.; Copéret, C.; Raynaud, C.; Eisenstein, O. *J. Am. Chem. Soc.* **2016**, 138, 2261-2272.
- (76) Yamamoto, K.; Gordon, C. P.; Liao, W.-C.; Copéret, C.; Raynaud, C.; Eisenstein, O. *Angew. Chem. Int. Ed.* **2017**, 56, 10127-10131.
- (77) Gordon, C. P.; Yamamoto, K.; Liao, W.-C.; Allouche, F.; Andersen, R. A.; Copéret, C.; Raynaud, C.; Eisenstein, O. *ACS Cent. Sci.* **2017**, 3, 759-768.
- (78) Helgaker, T.; Jaszuński, M.; Ruud, K. *Chem. Rev.* **1999**, 99, 293-352.
- (79) Kaupp, M.; Bühl, M.; Malkin, V. G., *Calculation of NMR and EPR Parameters: Theory and Applications*. Wiley-VCH: Weinheim, 2004.
- (80) Bohmann, J. A.; Weinhold, F.; Farrar, T. C. *J. Chem. Phys.* **1997**, 107, 1173-1184.
- (81) Autschbach, J. *J. Chem. Phys.* **2008**, 128, 164112.
- (82) Aquino, F.; Pritchard, B.; Autschbach, J. *J. Chem. Theory Comput.* **2012**, 8, 598-609.
- (83) Wu, G.; Rovnyak, D.; Johnson, M. J. A.; Zanetti, N. C.; Musaev, D. G.; Morokuma, K.; Schrock, R. R.; Griffin, R. G.; Cummins, C. C. *J. Am. Chem. Soc.* **1996**, 118, 10654-10655.

- (84) Ruiz-Morales, Y.; Schreckenbach, G.; Ziegler, T. *Organometallics* **1996**, *15*, 3920-3923.
- (85) Ruiz-Morales, Y.; Schreckenbach, G.; Ziegler, T. *J. Phys. Chem.* **1996**, *100*, 3359-3367.
- (86) Wiberg, K. B.; Hammer, J. D.; Zilm, K. W.; Cheeseman, J. R. *J. Org. Chem.* **1999**, *64*, 6394-6400.
- (87) Auer, D.; Strohmman, C.; Arbuznikov, A. V.; Kaupp, M. *Organometallics* **2003**, *22*, 2442-2449.
- (88) Sceats, E. L.; Figueroa, J. S.; Cummins, C. C.; Loening, N. M.; Van der Wel, P.; Griffin, R. G. *Polyhedron* **2004**, *23*, 2751-2768.
- (89) Auer, D.; Kaupp, M.; Strohmman, C. *Organometallics* **2004**, *23*, 3647-3655.
- (90) Auer, D.; Kaupp, M.; Strohmman, C. *Organometallics* **2005**, *24*, 6331-6337.
- (91) Karni, M.; Apeloig, Y.; Takagi, N.; Nagase, S. *Organometallics* **2005**, *24*, 6319-6330.
- (92) Kravchenko, V.; Kinjo, R.; Sekiguchi, A.; Ichinohe, M.; West, R.; Balazs, Y. S.; Schmidt, A.; Karni, M.; Apeloig, Y. *J. Am. Chem. Soc.* **2006**, *128*, 14472-14473.
- (93) Epping, J. D.; Yao, S.; Karni, M.; Apeloig, Y.; Driess, M. *J. Am. Chem. Soc.* **2010**, *132*, 5443-5455.
- (94) Standara, S.; Bouzkova, K.; Straka, M.; Zacharova, Z.; Hocek, M.; Marek, J.; Marek, R. *Phys. Chem. Chem. Phys.* **2011**, *13*, 15854-15864.
- (95) Zhu, J.; Kurahashi, T.; Fujii, H.; Wu, G. *Chem. Sci.* **2012**, *3*, 391-397.
- (96) Toušek, J.; Straka, M.; Sklenář, V.; Marek, R. *J. Phys. Chem. A* **2013**, *117*, 661-669.
- (97) Pascual-Borras, M.; Lopez, X.; Rodriguez-Forteza, A.; Errington, R. J.; Poblet, J. M. *Chem. Sci.* **2014**, *5*, 2031-2042.
- (98) Vícha, J.; Straka, M.; Munzarová, M. L.; Marek, R. *J. Chem. Theory Comput.* **2014**, *10*, 1489-1499.
- (99) Pascual-Borras, M.; Lopez, X.; Poblet, J. M. *Phys. Chem. Chem. Phys.* **2015**, *17*, 8723-8731.

- (100) Vummaleti, S. V. C.; Nelson, D. J.; Poater, A.; Gomez-Suarez, A.; Cordes, D. B.; Slawin, A. M. Z.; Nolan, S. P.; Cavallo, L. *Chem. Sci.* **2015**, *6*, 1895-1904.
- (101) Marchione, D.; Izquierdo, M. A.; Bistoni, G.; Havenith, R. W. A.; Macchioni, A.; Zuccaccia, D.; Tarantelli, F.; Belpassi, L. *Chem. Eur. J.* **2017**, *23*, 2722-2728.
- (102) Engl, P. S.; Santiago, C. B.; Gordon, C. P.; Liao, W.-C.; Fedorov, A.; Copéret, C.; Sigman, M. S.; Togni, A. *J. Am. Chem. Soc.* **2017**, *139*, 13117-13125.
- (103) Lenthe, E. v.; Baerends, E. J.; Snijders, J. G. *J. Chem. Phys.* **1993**, *99*, 4597-4610.
- (104) Lenthe, E. v.; Baerends, E. J.; Snijders, J. G. *J. Chem. Phys.* **1994**, *101*, 9783-9792.
- (105) Lenthe, E. v.; Snijders, J. G.; Baerends, E. J. *J. Chem. Phys.* **1996**, *105*, 6505-6516.
- (106) van Lenthe, E.; van Leeuwen, R.; Baerends, E. J.; Snijders, J. G. *Int. J. Quantum Chem.* **1996**, *57*, 281-293.
- (107) Lenthe, E. v.; Ehlers, A.; Baerends, E.-J. *J. Chem. Phys.* **1999**, *110*, 8943-8953.
- (108) Adamo, C.; Barone, V. *J. Chem. Phys.* **1999**, *110*, 6158-6170.
- (109) Mougél, V.; Copéret, C. *Chem. Sci.* **2014**, *5*, 2475-2481.
- (110) Mougél, V.; Santiago, C. B.; Zhizhko, P. A.; Bess, E. N.; Varga, J.; Frater, G.; Sigman, M. S.; Copéret, C. *J. Am. Chem. Soc.* **2015**, *137*, 6699-6704.
- (111) Jensen, F. *J. Chem. Theory Comput.* **2014**, *10*, 1074-1085.
- (112) Dolg, M.; Wedig, U.; Stoll, H.; Preuss, H. *J. Chem. Phys.* **1987**, *86*, 866-872.
- (113) Andrae, D.; Häußermann, U.; Dolg, M.; Stoll, H.; Preuß, H. *Theor. Chim. Acta.* **1990**, *77*, 123-141.
- (114) Martin, J. M. L.; Sundermann, A. *J. Chem. Phys.* **2001**, *114*, 3408-3420.

(115) Grimme, S.; Antony, J.; Ehrlich, S.; Krieg, H. *J. Chem. Phys.* **2010**, *132*, 154104.

(116) Marenich, A. V.; Cramer, C. J.; Truhlar, D. G. *J. Phys. Chem. B* **2009**, *113*, 6378-6396.

(117) Copéret, C.; Liao, W.-C.; Gordon, C. P.; Ong, T.-C. *J. Am. Chem. Soc.* **2017**, *139*, 10588-10596.